Postprint: Feng C, Janssen H. 2021. Hygric properties of porous building materials (VII): full-range benchmark characterizations of three materials, *Building and Environment*, 195:107727.
doi: https://doi.org/10.1016/j.jobe.2021.102284

Hygric properties of porous building materials (VII): full-range benchmark characterizations of three materials

Chi Feng[1,2,*], Hans Janssen[3]

1. School of Architecture and Urban Planning, Chongqing University, 400045 Chongqing, PR China
2. Key Laboratory of New Technology for Construction of Cities in Mountain Area, Chongqing University, 400045 Chongqing, PR China
3. KU Leuven, Department of Civil Engineering, Building Physics and Sustainable Design, 3001 Leuven, Belgium

Abstract: Material properties are requisite for all coupled heat and moisture transfer analysis, crucial to obtain clear insight into and optimized control of the hygrothermal processes in building envelopes and the built environment. Unfortunately, current databases and reported studies fail to provide the hygric properties of porous building materials exhaustively. This study characterized the hygric properties of three porous building materials – calcium silicate, autoclaved aerated concrete and ceramic brick. Standardized experimental methods were combined with recent novel techniques. All important moisture storage and transport properties were obtained, for the full humidity range, for both absorption and desorption. This completeness makes this data set valuable to the scientific community. The results can be used as material data in hygrothermal simulations and as experimental benchmarks for the validation of material models.
Keywords: porous building material; moisture storage; moisture transport; full humidity range; benchmark measurement

1. Introduction

1.1 Background

Heat and moisture transfer in porous building materials has a crucial impact on the energy efficiency of buildings [1], the service life and structural safety of components [2], as well as the indoor climate and the occupants' health [3]. The analysis of such transfer processes has therefore become one of the central issues of buildings and the built environment, with the aim of understanding, controlling and optimizing related aspects.

In the 1950s, Glaser [4] brought his famous 1-D steady-state vapor diffusion model, which analyzed the heat and vapor transfer in building envelopes with focus on the interstitial condensation. Because of its simplicity and clarity, today Glaser's model remains popular at both international and national levels. It is also adopted in many standards, such as the ISO 13788 standard [5] and the Chinese GB 50176 standard [6]. Unfortunately, due to its over-simplified assumptions, Glaser's model has many drawbacks and limitations, proved by numerous scientific research and engineering practice.

Also in the 1950s, Philip and De Vries [7, 8] introduced their coupled heat and moisture transfer model for porous materials. Since then many scholars have established their hygrothermal models. By 2013, there had been at least 50 hygrothermal models for analyzing the heat and moisture transfer in porous building materials or building envelopes [9], while at the whole building level more than 15 models had been constructed [10]. These hygrothermal models are physically more reasonable but also

numerically more complicated than Glaser's model. Their essence is a set of coupled partial differential equations, describing heat and moisture transfer processes, respectively. Although the number of hygrothermal models seems overwhelming, it can be shown that they are mathematically convertible [11], with two core input parameter sets shared by all, being the boundary conditions and the material properties. In this series we focus on material properties.

1.2 Material properties in a nutshell

In all hygrothermal models, material properties are indispensable input information. Typically, they are grouped as thermal properties (e.g. the thermal conductivity) and hygric properties (e.g. the vapor permeability) [12], representing a material's characteristics related to heat and moisture respectively. Of all these properties, bulk density (ρ_{bulk}, kg·m^{-3}) and open porosity (ϕ, -) are the most fundamental. Since they are closely related to both thermal and hygric processes, they can be classified into either group. Thermal properties are in general physically straightforward to understand, mathematically simple to depict, and experimentally easy to obtain. On the contrary, hygric properties are often more complicated in all these aspects.

Hygric properties can be further classified as moisture storage and transport properties [13]. Storage properties describe how much moisture a material can store at a given condition, typically including saturated moisture content (w_{sat}, kg·m^{-3}), capillary moisture content (w_{cap}, kg·m^{-3}), sorption isotherms (moisture content (w, kg·m^{-3}) as a function of relative humidity) and retention curves (moisture content as a function of capillary pressure (p_c, Pa)). Transport properties, on the other hand, characterize how easy water vapor and liquid water can be transported in a material, often comprising capillary absorption coefficient (A_{cap}, kg·m^{-2}s$^{-0.5}$), vapor permeability (often expressed in terms of the resistance factor (μ, -)), liquid permeability (K_l, kg·m^{-1}s^{-1}Pa^{-1}) and liquid diffusivity (D_l, m^2·s^{-1}). Their detailed definitions are available in ref. [13-20], and we do not repeat these here.

One important and intricate feature of hygric properties is that due to capillary hysteresis, many hygric properties depend not only on the ambient environment but also on the (de)saturation process. In other words, even if the specific environmental conditions remain unchanged, a storage or transport property can still be different for varied absorption or desorption processes. The most typical example is that different curves are needed to characterize the moisture storage for absorption and desorption processes, as illustrated in Fig.1 [13]. The complexity also exists for moisture transport. For instance, liquid permeability can often be approximated by a single curve [21] (Fig.2), and its relationship with liquid diffusivity is:

$$D_l = \frac{K_l}{dw/dp_c} \tag{1}$$

Since dw/dp_c – the slope of moisture retention curve – is process-dependent, the liquid diffusivity may hence also be process-dependent.

Currently, there are three typical methods to obtain hygric properties. The first method is physical modeling. For instance, with a pore-structure-based model hygric properties of porous building materials can be directly predicted [22]. The second method is inverse modeling. Based on monitored hygrothermal processes and a pre-defined hygrothermal model, material properties can also be determined [23]. The last and most popular method is direct measurement. By far many experimental protocols have been established and standardized for measuring hygric properties, such as those mentioned in Section 2.2.

The experimental determination of hygric properties has been applied widely for decades. However, the dependability and capability challenges are still not overcome yet [12]. The dependability challenge

refers to the experimental results not always being reliable. An example is that different labs using the same experimental protocol on the same material fail to provide similar results, as happened in many round robin campaigns [12, 24]. The capability challenge exists because of hysteresis and other factors, causing traditional experimental methods failing to cover the full humidity range for both absorption and desorption processes. Researchers have been consistently confronting this challenge by innovating original experimental methods [13, 25-27], but this is still a work in progress.

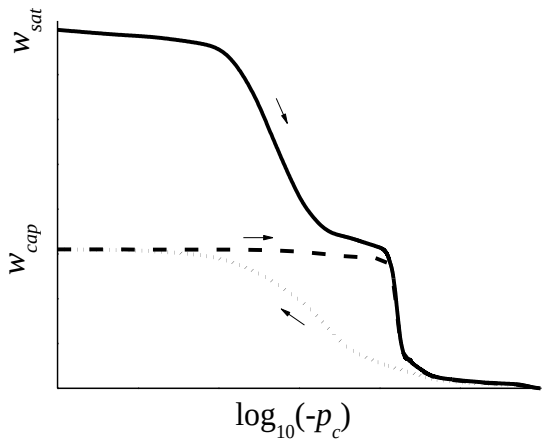

Fig.1 Moisture retention curves [13]

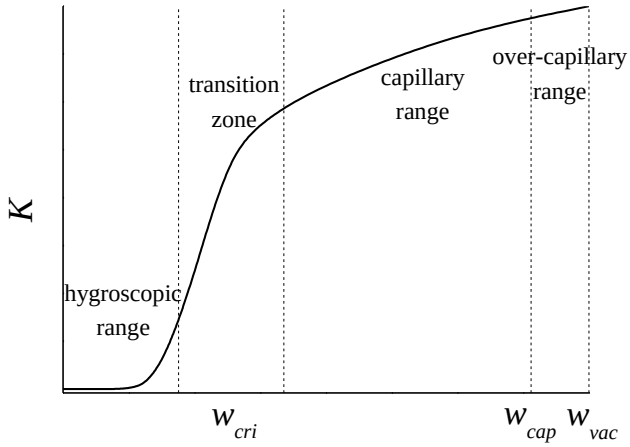

Fig.2 A typical liquid permeability curve

Table 1 Measured hygric properties in some recent experimental publications

Researcher(s)	Zhao and Plagge [28]	Huang *et al* [29]	Haba *et al* [30]	Kočí *et al* [31]	Jerman *et al* [32]	Seng *et al* [33]	Colinart *et al* [34]
Year	2015	2017	2017	2019	2019	2019	2020
Target material(s)	Sandstones	Bamboos	Data palm concrete	Aerated concrete	Bio-materials	Hemp concrete	Hemp clay
ρ_{bulk}	√	√	√	√	√	√	√
ϕ or w_{sat}	√	√	√	√	√	√	√
w_{cap}	√	√	×	×	√	×	×
Sorption isotherm (absorption)	√	√	√	×	√	√	√
Sorption isotherm (desorption from w_{sat})	√ [a]	√ [a]	×	×	×	√ [b]	×
Sorption isotherm (desorption from w_{cap})	- [a]	- [a]	×	×	×	×	×
Retention curve (absorption)	×	×	×	×	×	×	×
Retention curve (desorption from w_{sat})	√ [a]	×	×	×	×	×	×
Retention curve (desorption from w_{cap})	- [a]	×	×	×	×	×	×
A_{cap}	√	√	√	×	√	√	√
μ	√	√	√	√	√	√	√
K_l	√	×	×	×	×	×	×
D_l (absorption)	×	×	×	√	√ [c]	√ [c]	×
D_l (desorption from w_{sat})	×	×	×	×	×	×	×
D_l (desorption from w_{cap})	×	×	×	×	×	×	×

a. It is not clear whether the desorption tests started from w_{sat}, w_{cap} or others;
b. From RH 97%;
c. Estimated from other properties as a single value.

Table 1 summarizes some recent material property measurements. These studies are of high quality and provide very valuable information. However, none of them covers the full-range hygric properties. In fact, all available databases for the hygrothermal properties of porous building materials – such as ref. [19, 20] – fail to provide all the aforementioned hygric properties (note that we only need either ϕ or w_{sat}, and either K_l or D_l). Due to the dependability challenge, previously reported material properties are not free from great uncertainties, either. Consequently, the physical and statistical models for hygric property determination cannot be fully verified at present, implying that other theoretical or practical applications of hygrothermal models are also subject to doubts.

1.3 Objectives

This campaign characterized all important hygric properties of three porous building materials, by dependable experiments over the full humidity range for both absorption and desorption processes. These data can be used as benchmarks for various purposes, like the validation of material models. In the following sections, the target materials and the test methods are introduced first. After that, the experimental results are presented in detail and analyzed in depth.

2. Materials and methods

2.1 Materials

In this study, we resorted to the materials selected in many hygric property tests [14-16, 24]: calcium silicate (CS), autoclaved aerated concrete (AAC) and ceramic brick (CB). The pore size distributions of these materials were determined from the mercury intrusion porosimetry [35, 36], and the results are illustrated in Fig.3. Since small pores mainly determine the hygroscopicity of a material while large pores are more closely related to the capillarity, we can expect that CS is high in hygroscopicity and capillarity, AAC is high in hygroscopicity but low in capillarity, and CB is high in capillarity but low in hygroscopicity. These speculations are verified in the following sections with experimental results, and the general variations of the hygric performance of selected materials hence cover the typical combinations of hygric characteristics; do note that it is not very valuable to test a material low in both hygroscopicity and capillarity.

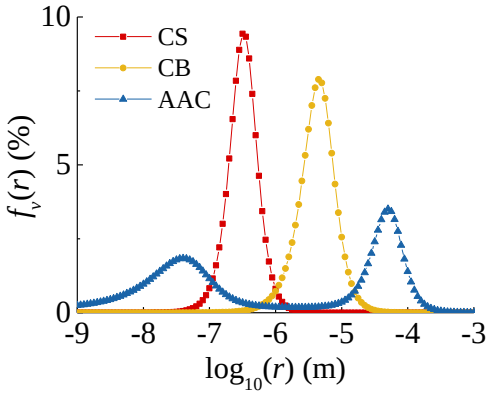

Fig.3 The pore size distributions of the target materials

2.2 Test Methods

For our benchmark purpose, the measured hygric properties must satisfy two criteria:

a) The full humidity range for both absorption and desorption processes must be covered;
b) The experimental results must be reliable.

To satisfy the first criterion, we applied not only the traditional and standardized test methods but

also some recently developed novel experimental protocols. To meet the second requirement, we performed multiple experiments to repeatedly determine the same hygric property whenever possible or necessary. The underlying logic is that if different methods provide similar results, it is highly plausible that all results are trustworthy because the systematic errors from different methods are unlikely the same. In general, all measurements were performed at 22-23°C unless otherwise specified. The dimensions of all samples were measured with calipers reading 0.01 mm, while the mass was measured to 0.001 g with an electronic balance. For the dry mass determination, samples were first dried at 70°C in a ventilated oven supplied with compressed air for at least 7 days. Other detailed experimental procedures are explained below. The setups are illustrated in Fig.4.

a) Vacuum saturation test

b) Mercury intrusion test

c) Pressure plate test

d) Modified pressure plate test

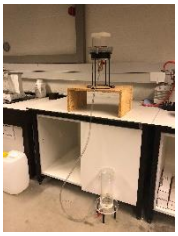

e) Water column test

f) Semi-permeable membrane test

g) Psychrometer test

h) Desiccator test

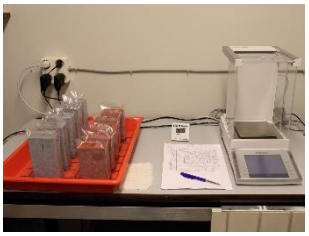

i) Capillary absorption test

j) Cup test

k) X-ray attenuation test

l) Falling water head test

Fig.4 Photos of the experimental setups
(not necessarily the measurements in this study)

It should be noted that the judgment on the hygric equilibrium is of vital importance, especially for those moisture storage tests. In general, tests with liquid transfer (e.g. the water column test) can reach equilibrium much faster than those going through vapor diffusion (e.g. the desiccator test) due to

smaller internal and boundary resistance for liquid transfer. There are many impact factors, such as material characteristics, sample sizes, moisture transfer process and so on. It is therefore difficult to impose a universal criterion on the hygric equilibrium determination for all tests. To avoid interference in the formal measurements, the best strategy is to conduct trial measurements in advance. One criterion could be that when 3 successive weighings (at time intervals of 1-2 days) indicate a limited mass change (e.g. within 0.1% fluctuation), hygric equilibrium can be considered to have been reached. Another method is to measure the moisture potential in the sample with a psychrometer and compare that with the exerted boundary condition. If these two values are the same, equilibrium can also be deemed reached. In this study we adopted both methods whenever applicable, and the agreement of results from different methods also confirmed the equilibrium indirectly.

2.2.1 Basic tests

- Vacuum saturation test

The vacuum saturation test was performed to determine the bulk density, open porosity and saturated moisture content. Our experimental procedures were based on the ISO 10545-3 [37], ASTM C1699 [38] and ASTM C642 [39] standards, as well as adopted from Ref. [16]. Samples had a diameter of 5 cm and a thickness of 0.5 cm, and four duplicates were used for each material. During the test, dry samples were first put in a vacuum container wherein the air pressure was maintained below 3000 Pa by a vacuum pump. Samples were stored there for at least 4 h to completely evacuate the air inside. Then distilled water was slowly supplied with the vacuum pump running, causing the water level in the container to rise at a rate of around 5 cm/h. When all samples were completely submerged, the water supply was stopped and the air pressure in the container was returned to the atmospheric pressure. One day later, the samples were weighed both in the air and under water. The bulk density, open porosity and saturated moisture content were then calculated by the Archimedes' law.

- Mercury intrusion test

The mercury intrusion test was performed to determine the pore volume distribution, which was also converted to the desorption retention curve starting from w_{sat} with the help of the Kelvin-Laplace equation. Our experimental procedures were based on the ISO 15901-1 [35] and ASTM D4404 [36] standards, as well as adopted from Ref. [40]. Samples had a size of roughly $2\times1\times1$ cm^3. Since the mercury intrusion test was not highly reliable and the results were just for semi-quantitative reference, only one sample was used for each material. The test was automatically run by an AutoPore IV mercury porosimeter (producer: Micromeritics®). The applied pressure gradually went up from 0 to $2\cdot10^8$ Pa, with a 120 s equilibrium period for each pressure step.

2.2.2 Storage tests

- Pressure plate test

The pressure plate test was performed to determine the moisture retention curve for the desorption process. Our experimental procedures were based on the ISO 11274 [41], ASTM C1699 [38] and ASTM D6836 [42] standards, as well as adopted from our previous study [16]. Samples had a diameter of 5 cm and a thickness of 0.5 cm, and four duplicates were used for each material. During the test, samples were first pre-conditioned to saturated or capillary moisture content. Next, they were laid on a saturated porous ceramic plate in the pressure vessel. Between the samples and the plate, moist kaolin was used to maintain hydraulic contact, with a thin cellulose film for contamination prevention. After that compressed air was let into the sealed pressure vessel to force the water in the samples out, flowing through the porous ceramic plate. The applied air pressure corresponded to the target capillary pressure, stepwise increasing to $1.25\cdot10^4$, $2.5\cdot10^4$, $5\cdot10^4$, $1\cdot10^5$, $1.5\cdot10^5$, $2\cdot10^5$, $3\cdot10^5$, $5\cdot10^5$, $7\cdot10^5$, $1\cdot10^6$ and

$1.5 \cdot 10^6$ Pa. For each pressure step, the wet mass of samples was measured when equilibrium was reached (after approximately 1-2 weeks). The moisture content was hence available.

- Modified pressure plate test

The modified pressure plate test was performed to determine the moisture retention curve for the absorption process. This method was recently proposed by the authors of this study [26]. Samples also had a diameter of 5 cm and a thickness of 0.5 cm, and four duplicates were used for each material. The overall setup was similar to that of the traditional pressure plate, except that the water outflow tube of the pressure vessel was connected to a filled water tank, and that a piece of moist filter paper replaced the kaolin and cellulose film between the samples and the porous ceramic plate. During the test, dry samples were used and an air pressure higher than the target was applied first. After 1-2 h the air pressure in the pressure vessel was slowly decreased to the target value ($1.1 \cdot 10^6$, $8 \cdot 10^5$, $5 \cdot 10^5$, $3 \cdot 10^5$, $2 \cdot 10^5$ and $1 \cdot 10^5$ Pa), forming a suction and a continuous water supply from the water outlet into the pressure vessel. Samples hence absorbed water at this pressure until equilibrium was reached (after approximately 3-4 weeks). The moisture content of the samples was then determined gravimetrically.

- Water column test

The water column test was performed to determine the moisture retention curve for the desorption process at capillary pressures close to 0 Pa. Our experimental procedures were based on the ISO 11274 [41] and ASTM D6836 [42] standards, as well as adopted from Ref. [43]. Samples had a diameter of 5 cm and a thickness of 0.5 cm, and four duplicates were used for each material. During the test, samples were first pre-conditioned to saturated or capillary moisture content. Next, they were laid on a saturated porous ceramic plate in a sealed container, with a piece of moist filter paper in between. Unlike the pressure plate test where compressed air was applied above the porous ceramic plate, a water column was hung below the porous ceramic plate for pressure control in this test. By changing the height of the water column, the suction pressure exerted on the porous ceramic plate (and hence on the samples) could be regulated. The applied suction pressure increased stepwisely for $2 \cdot 10^3$, $4 \cdot 10^3$, $8 \cdot 10^3$ and $1.25 \cdot 10^4$ Pa. After reaching equilibrium (1-2 d), the moisture content of samples was determined gravimetrically.

- Semi-permeable membrane test

The semi-permeable membrane test was performed to determine the moisture retention curve for both absorption and desorption processes. This method was recently proposed by the authors of this study [13]. Samples had a diameter of 3 cm and a thickness of 0.5 cm, and four duplicates were used for each material under each humidity condition. During the test, samples were either dried or pre-conditioned to saturated or capillary moisture content. They were laid on the bottom of a sample holder, made of a piece of reverse osmosis membrane (Filmtech® Flat Sheet BW30). The other side of the semi-permeable membrane was in direct contact with an unsaturated K_2SO_4 solution, providing a fixed osmotic pressure. By preparing K_2SO_4 solutions of different concentrations, applied osmotic pressures varied from $-2 \cdot 10^5$ to $-3.2 \cdot 10^6$ Pa, corresponding to different capillary pressures. In total eight evenly-distributed humidity conditions were maintained, and tests were performed simultaneously in different setups. After reaching equilibrium (3-4 weeks), the moisture content of samples was determined gravimetrically.

- Psychrometer test

The psychrometer test was performed to determine the moisture retention curve for both absorption and desorption processes. This method was proposed by the authors of this study together with the semi-permeable membrane test [13]. Samples also had a diameter of 3 cm and a thickness of 0.5 cm,

and 20-30 duplicates were used for each material. During the desorption test, samples were first pre-conditioned to saturated or capillary moisture content. Next, they were put into different containers with RH 97% or 94% inside (controlled by saturated K_2SO_4/KNO_3 solutions). From time to time, samples in different containers were interrupted from the desorption process by sealing into small sample cups. After a standing period of 15-20 h, the moisture distributions in the samples were assumed uniform. Then a WP4C dewpoint psychrometer was used to measured the capillary pressure in each sample, and the moisture content was determined gravimetrically. After that, samples were returned to containers for further desorption. The absorption test was similar, except that dry samples were initially pre-conditioned to equilibrium at RH 97% and then started absorption by exposing to an ambient RH of 100% (above pure water).

- Desiccator test

The desiccator test was performed to determine the sorption isotherms for both absorption and desorption processes. Our experimental procedures were based on the ISO 12571 [44] and ASTM C1498 [45] standards, as well as adopted from Ref. [18]. Samples had a diameter of 5 cm and a thickness of 0.5 cm, and four duplicates were used for each material under each RH. During the test, samples were either dried or pre-conditioned to saturated or capillary moisture content. Next, they were put into different desiccators with varied RHs inside. In total seven saturated salt solutions were used, namely LiCl, $MgCl_2$, $Mg(NO_3)_2$, NaCl, KCl, KNO_3 and K_2SO_4, producing RHs of 11.3%, 32.9%, 53.5%, 75.4%, 84.7%, 94.0% and 97.4%, respectively. After reaching equilibrium (1-2 months), the moisture content of samples was determined gravimetrically.

2.2.3 Transport tests

- Capillary absorption test

The capillary absorption test was performed to determine the capillary absorption coefficient and capillary moisture content. Our experimental procedures were based on the ISO 15148 [46] and ASTM C1794 [47] standards, as well as adopted from Ref. [15]. Samples had a bottom size of 8 cm×4 cm and a height of 12 cm (CS and CB) or 6 cm (AAC). Four duplicates were used for each material. Before the test, the lateral sides and the top of dry samples were sealed by plastic films, with the bottom 1 cm of the lateral sides unwrapped and two small holes opened in the film on the top. Samples were then put in contact with distilled water for capillary absorption, with the bottom 3-5 mm below the water level. From time to time, samples were taken out of water for mass determination and then put back. Each weighing process was finished within 20 s. This process continued for hours (CS and CB) or days (AAC). For data processing, the absorbed water mass per bottom area was plotted as a function of the square root of time, and the overall process could be divided into a rapid-absorption process (the 1^{st} stage) and a slow-absorption process (the 2^{nd} stage). The slope of the 1^{st} stage was calculated as the capillary absorption coefficient, while the moisture content at the cross point of the 1^{st} and the 2^{nd} stages was calculated as the capillary moisture content.

- Cup test

The cup test was performed to determine the vapor permeability (vapor diffusion resistance factor). Our experimental procedures were based on the ISO 12572 [48] and ASTM E96 [49] standards, as well as adopted from Ref. [16]. Samples had a diameter of 10 cm and a thickness of 4 cm for CS and AAC, or a diameter of 8 cm and a thickness of 3 cm for CB. Four duplicates were used for each material under each RH. During the test, the samples were laterally sealed by epoxy first and then mounted on the opening of diffusion cups. The RHs in and out of the cups were controlled by saturated salt solutions. In total three RH pairs were used, namely 11.3%-53.5% (LiCl-$Mg(NO_3)_2$), 53.5%-84.7%

($Mg(NO_3)_2$-KCl) and 84.7%-97.4% (KCl-K_2SO_4). After an initial period of one week for reaching steady-state, the cups were weighed every 3-4 days for 7 times. The mass change was fitted linearly as a function of time, finally deriving the vapor permeability by the Fick's law, expressed as the vapor diffusion resistance factor. Note that there was no masked edge of the sample, and the resistance of the air layer inside the cup was corrected.

- X-ray attenuation test

The X-ray attenuation test was performed to determine the liquid diffusivity for the absorption process. It is widely used but not standardized yet. Our experimental procedures were adopted from Ref. [50]. Samples had a bottom size of 8 cm×2 cm and a height of 12 cm (CS and CB) or 3 cm (AAC). Considering the availability of the X-ray setup and the complexity of data processing, only two duplicates were used for each material. It was based on the standard capillary absorption test, except that only the 1st stage absorption was conducted, and that the sample was not regularly weighed. Instead, an X-ray setup was utilized to monitor the sample's transient moisture profile, based on the absorption of X-ray by the liquid water in the sample. With the help of Boltzmann transformation, the transient moisture profile was converted to a characteristic curve, finally providing the liquid diffusivity.

- Falling water head test

The falling water head test was performed to determine the liquid permeability. Our experimental procedures were based on the ISO 17892-11 [51] and ASTM D2434 [52] standards, as well as adopted from Ref. [53]. Samples had a diameter of 8 cm and a thickness of 2-4 cm. For each material 5-7 duplicates were repeatedly used. During the test, laterally sealed (by epoxy) samples were pre-conditioned to different moisture content between the capillary and saturated moisture content. Next, they were mounted on the water head setup, with a water column standing above. The gravity of the water column exerted a driven force, with the water head decreasing gradually as water flew through the sample. The water level was recorded regularly. With the Darcy's law, the liquid permeability was finally derived.

3. Results and discussion

In this section, we report the experimental results obtained from the tests mentioned above. For moisture storage and transport curves, discrete data points were also fitted into continuous curves.

3.1 Single-valued hygric properties

Unlike the moisture storage and transport curves, some hygric properties are single-valued when the influence of temperature and other impacts (e.g. air pressure) are neglected. Table 2 summarizes these properties of all three target materials. The large A_{cap} values of CS and CB, as well as their closeness between w_{cap} and w_{sat}, are closely related to their large pores, reflecting their high capillarity. AAC, restricted by its small pores, contrarily showed low capillarity.

Table 2 The single-valued hygric properties of target materials [a]

Properties	CS	AAC	CB
ρ_{bulk} (kg·m^{-3})	271.0 (1.5)	461.2 (9.0)	1818.3 (32.0)
ϕ (%)	89.1 (0.2)	81.4 (0.5)	32.6 (0.4)
w_{sat} (kg·m^{-3})	888.8 (2.5)	812.6 (4.6)	325.6 (3.5)
w_{cap} (kg·m^{-3})	755.8 (2.3)	313.4 (11.6)	209.6 (4.5)
A_{cap} [b] (kg·m^{-2}s$^{-0.5}$)	1.01 (0.01)	0.046 (0.005)	0.607 (0.020)

a. The values in brackets are the standard deviations from four duplicate samples;
b. Values at 20°C.

3.2 Moisture storage curves

The experimental data points for CS in the desorption process starting from w_{sat} are illustrated in Fig.5 as an example (for other processes and materials please refer to Appendix A). These were obtained from multiple methods in the full humidity range. It should be noted that these data were plotted as functions of both p_c and RH. Since p_c and RH are linked by the Kelvin-Laplace equation, moisture retention curves and sorption isotherms are therefore mutually convertible, both describing the moisture storage capacity of a material. However, due to different expression accuracies, sorption isotherms are more frequently used in the hygroscopic range while the moisture retention curves are the counterparts in the capillary range.

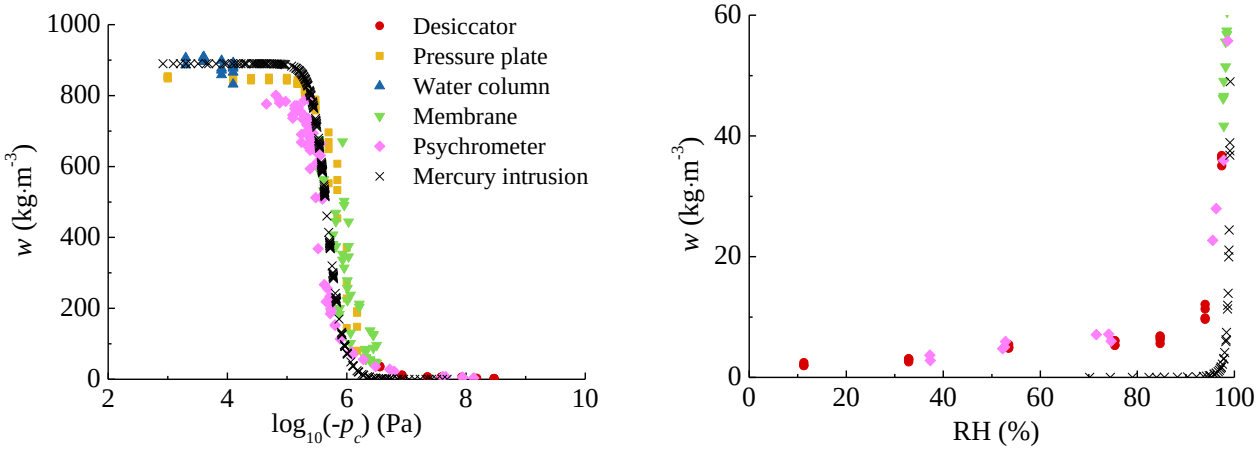

a) Moisture retention curve b) Sorption isotherm

Fig.5 Experimental results for the moisture storage curves of CS (desorption from w_{sat})

It is clearly revealed in Fig.5 that the results obtained from different methods agreed nicely in the full humidity range. There were inevitably some minor scatters, but this was expected because different methods have their own systematic and random errors. It should be noted that the mercury intrusion test significantly deviated from other results in the hygroscopic range. This may be attributed to the calibration, the choice of the contact angle, the compression under high pressures and other factors [40, 54, 55]. Consequently, we only used the mercury intrusion results as a reference but did not include them in the data processing.

For practical use, it is convenient to fit the discrete experimental points into continuous curves, covering the full humidity range and depicting respective absorption/desorption processes. For this purpose, we modified the classic van Genuchten model [56] into Eq.(2):

$$w = w_0 \cdot \sum_{i=1}^{n} l_i \left[1 + (k_1^i \cdot \log_{10} p_c)^{k_2^i}\right]^{\frac{1-k_2^i}{k_2^i}} \tag{2}$$

where k_1 - k_3 were all fitting parameters. In Eq.(2) the fitting parameter w_0 should be w_{sat} for the desorption curve starting from w_{sat}, and w_{cap} for the desorption curve from w_{cap} and the absorption curve from the dry state. The parameter l_i was the weighing factor for system i constrained by $\sum_{i=1}^{k} l_i = 1$. As reflected in Fig.3, CS and CB had only one pore system so their n value was 1, while AAC had two main pore sizes so its n value was fixed as 2.

Besides the moisture retention curves fitted with Eq.(2) covering the full humidity range, it is also desirable to have sorption isotherms for some applications in the hygroscopic range only (e.g. predicting the occurrence of interstitial condensation). Therefore we selected the data points below

97.4% RH and fitted them with our mathematical model proposed in ref. [18] for the sorption isotherms:

$$w = \ln\frac{(100\cdot\mathrm{RH}+1)^{k_1}}{(1-\mathrm{RH})^{k_2}} + k_3\cdot\exp(100\cdot\mathrm{RH}) \quad (3)$$

It should be mentioned that it is impossible to judge which experimental protocol is the best. Consequently, we assumed the overall results combining all measurements (except mercury intrusion) should be the most reliable. The fitted curves are illustrated in Fig.6 and the mathematical equations are summarized in Table 3. The moisture retention curves in Fig.6 corresponded to the pore structures of three materials clearly, as the rapid increase/decrease of moisture content at given capillary pressures were directly linked to pore sizes, prescribed by the Laplace equation. An interesting phenomenon from Fig.6 is that although there were some hysteresis effects between absorption and desorption curves, the two desorption curves starting from w_{sat} and w_{cap} came close and almost overlapped after decreasing to a certain humidity. Currently there are no physical explanations available, and further investigations are needed.

It should be noted that the sorption isotherms of CB were not reliable due to its very low hygroscopicity, as predicted from its large pore size (Fig.3). For this reason, its desorption isotherm starting from w_{cap} was not measured. In addition, its moisture retention curve for the absorption process stayed slightly above the desorption curve starting from w_{cap}, which was physically impossible. The main reason should be that CB has low hygroscopicity but high capillarity, thus its absorption transition could be very sharp and resultantly difficult to detect. Limited by the accuracy of the absorption test methods in this transition range [13], its measurement uncertainties could be larger than the other two materials.

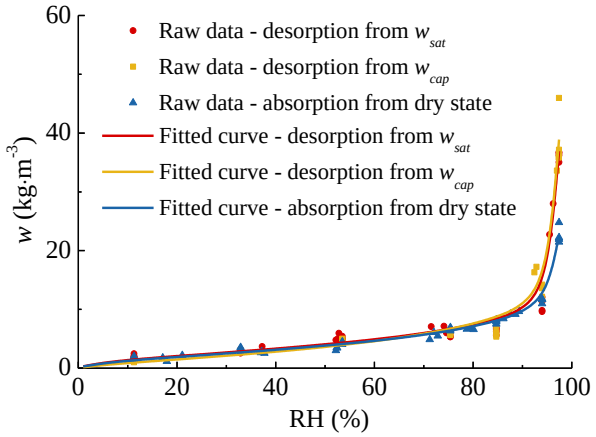

a) The sorption isotherms of CS

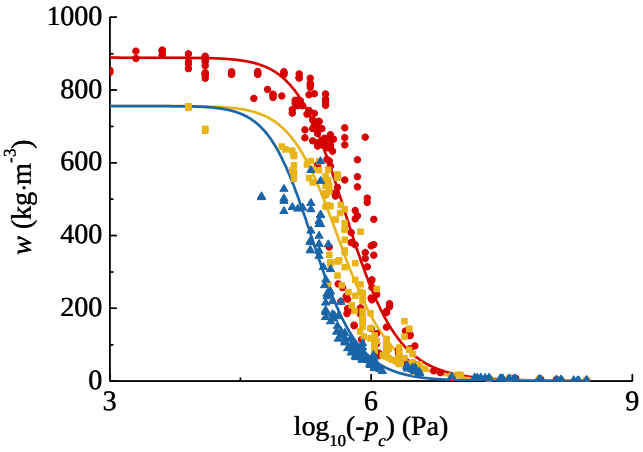

b) The moisture retention curves of CS

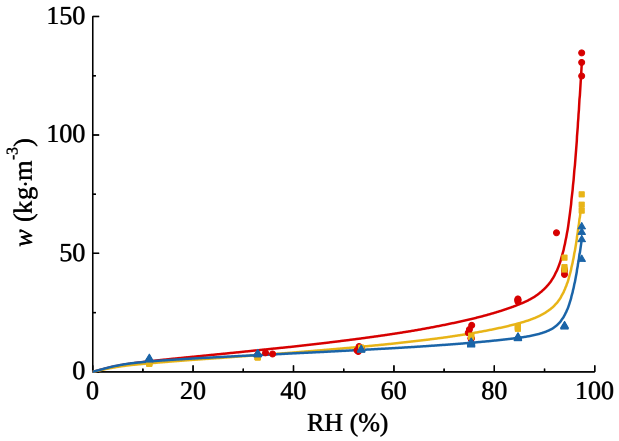

c) The sorption isotherms of AAC

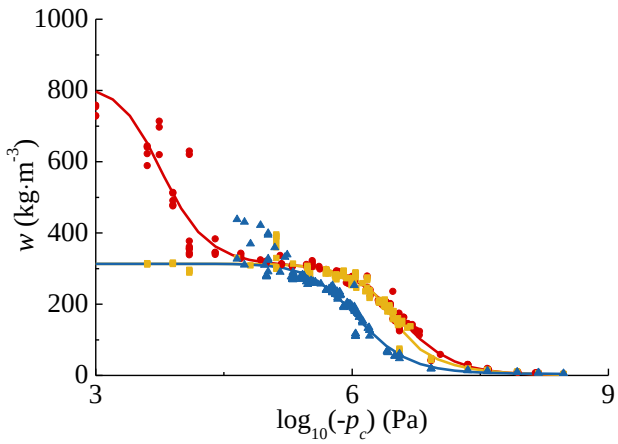

d) The moisture retention curves of AAC

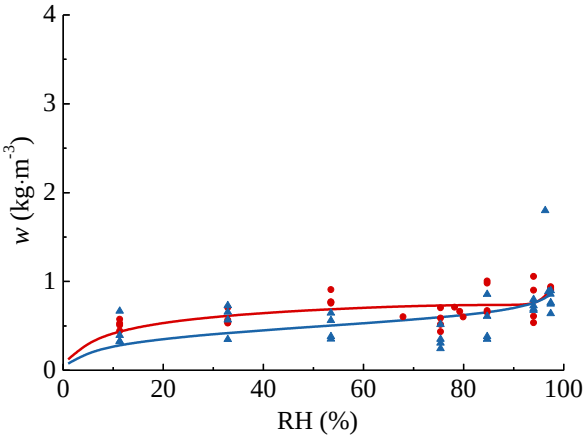

e) The sorption isotherms of CB

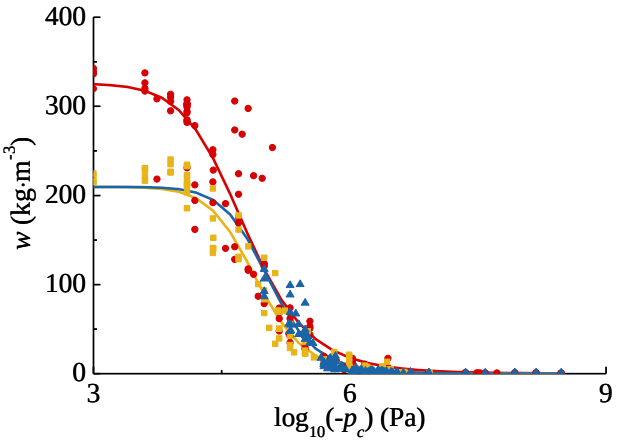

f) The moisture retention curves of CB

Fig.6 Fitted moisture storage curves of target materials

Table 3 Fitted moisture storage curves of target materials

Material		Moisture retention curve						Sorption isotherm			
		l_1	k_1^1	k_2^1	k_1^2	k_2^2	R^2 [a]	k_1	k_2	k_3	R^2
CS	Desorption from w_{sat}	1.0	0.175	20.46	-	-	0.93	0.421	3.462	$1.12\cdot10^{-41}$	0.96
	Desorption from w_{cap}	1.0	0.178	20.47	-	-	0.94	0.181	4.202	$1.14\cdot10^{-41}$	0.97
	Absorption from dry state	1.0	0.188	21.75	-	-	0.88	0.380	3.376	$4.28\cdot10^{-42}$	0.99
AAC	Desorption from w_{sat}	0.378	0.152	21.96	0.265	14.86	0.96	1.216	12.09	$4.02\cdot10^{-41}$	0.98
	Desorption from w_{cap}	0.35	0.154	52.64	0.154	18.38	0.96	1.061	8.27	$1.83\cdot10^{-41}$	0.97
	Absorption from dry state	0.99	0.165	20.95	$3.47\cdot10^{-4}$	7.31	0.94	1.697	3.61	$1.75\cdot10^{-41}$	0.98
CB	Desorption from w_{sat}	1.0	0.211	13.11	-	-	0.92	0.177	-0.028	$1.04\cdot10^{-43}$	0.35
	Desorption from w_{cap}	1.0	0.204	17.65	-	-	0.96	-	-	-	-
	Absorption from dry state	1.0	0.199	18.74	-	-	0.87	0.109	0.089	$1.42\cdot10^{-44}$	0.26

a. The coefficient of determination.

In short, porous building materials with small pores are high in hygroscopicity, reflected by their high moisture content for sorption isotherms. For materials with large pores, high capillarity can be expected, shown by the rapid change of moisture content when the ambient capillary pressure approaches 0 Pa.

3.3 Moisture transport curves

The cup test results are illustrated in Fig.7. The μ values of respective samples were plotted as a function of the average RH of their specific measurement conditions. Clearly, for all three materials their μ values decreased with rising RH. This is a common phenomenon observed in all cup tests, caused by the condensed water in the pores. For CB this trend was less obvious than the other two materials, reflecting its low hygroscopicity. More specifically, there were not many small pores in CB. The capillary condensation was therefore very weak, unable to form many water islets to facilitate vapor transfer.

As reflected in Fig.6, the hysteresis in the hygroscopic range was limited for all three materials, thus their cup test results could be expressed in terms of RH by Eq.(4). The fitted results are summarized in Table 4.

$$\mu = \frac{1}{k_1 + k_2 \cdot \mathrm{RH}^{k_3}} \tag{4}$$

In this study, we did not have an alternative method to verify the reliability of our cup test results. In a recent round robin campaign, however, we measured the equivalent resistance factor of CB and the results were in nice agreement with other labs [12], validating our cup tests.

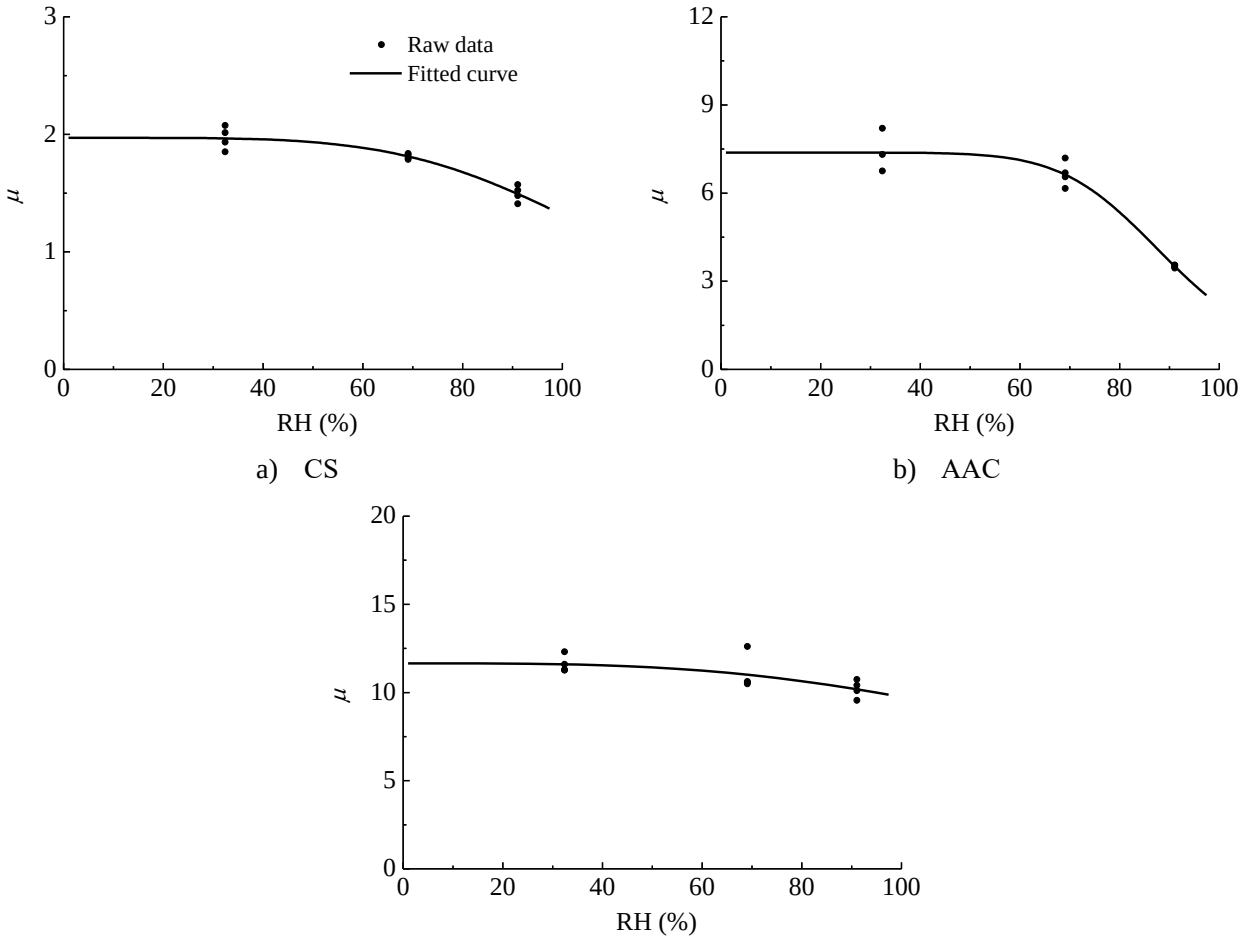

Fig.7 The vapor permeabilities of target materials

Fig.8a exemplifies the transient moisture profiles obtained by the X-ray attenuation method during the capillary absorption process of a CS sample. After Boltzmann transformation, the multiple moisture profiles were converted into a single *w*-*λ* profile (Fig.8b), which was then described with the following analytical expression [57]:

$$\lambda(w) = \frac{1}{k_1}\left[\tan\left(-\frac{w+w_{cap}}{k_2}\right) - k_3\right] \tag{5}$$

where λ was the Boltzmann variable ($m \cdot s^{-0.5}$) defined by:

$$\lambda = x/\sqrt{t} \tag{6}$$

where x was the distance (m) and t the time (s).

With the known expression of λ, the liquid diffusivity was calculated by:

$$D_l = -\frac{1}{2} \cdot \frac{\int_{w_0}^{w} \lambda dw}{\left(\frac{dw}{d\lambda}\right)_w} \tag{7}$$

where w_0 was the initial moisture content, $kg \cdot m^{-3}$. For our absorption case w_0 equated to 0.

The liquid diffusivity was finally approximated by the following expression:

$$\log_{10} D_l = k_1 + k_2 \cdot \exp\left(\frac{w}{k_3}\right) + k_4 \cdot \exp\left(\frac{w}{k_5}\right) \quad (8)$$

where k_1 - k_5 were fitting parameters. Fig.9 illustrates the w-λ profiles and the final liquid diffusivities of all target materials, with Table 4 summarizing the fitted diffusivity curves.

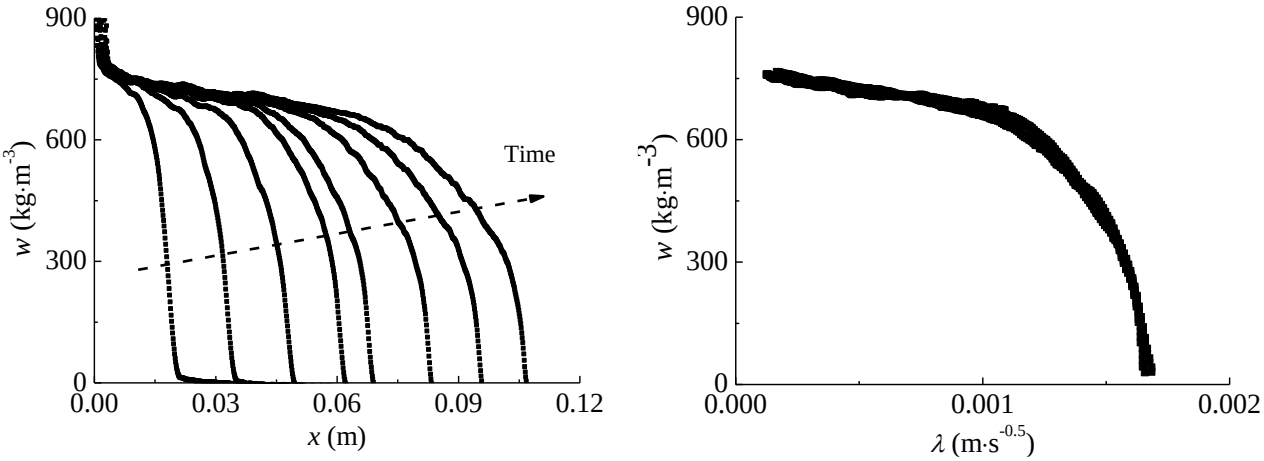

a) The transient moisture profiles b) The converted w-λ profile

Fig.8 The moisture content and w-λ profiles of a CS sample in the X-ray attenuation test

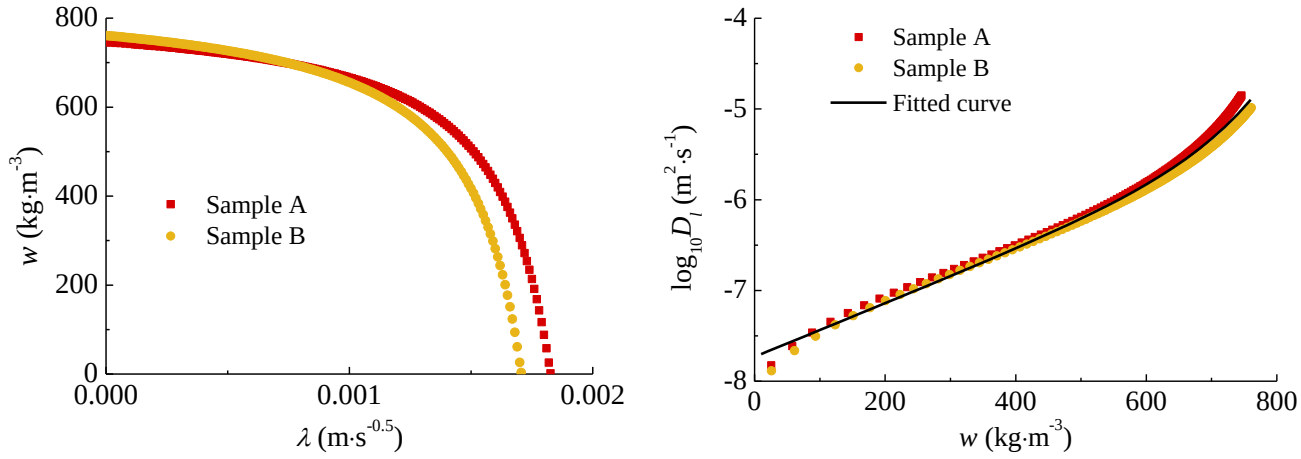

a) The w-λ profile of CS b) The liquid diffusivity of CS

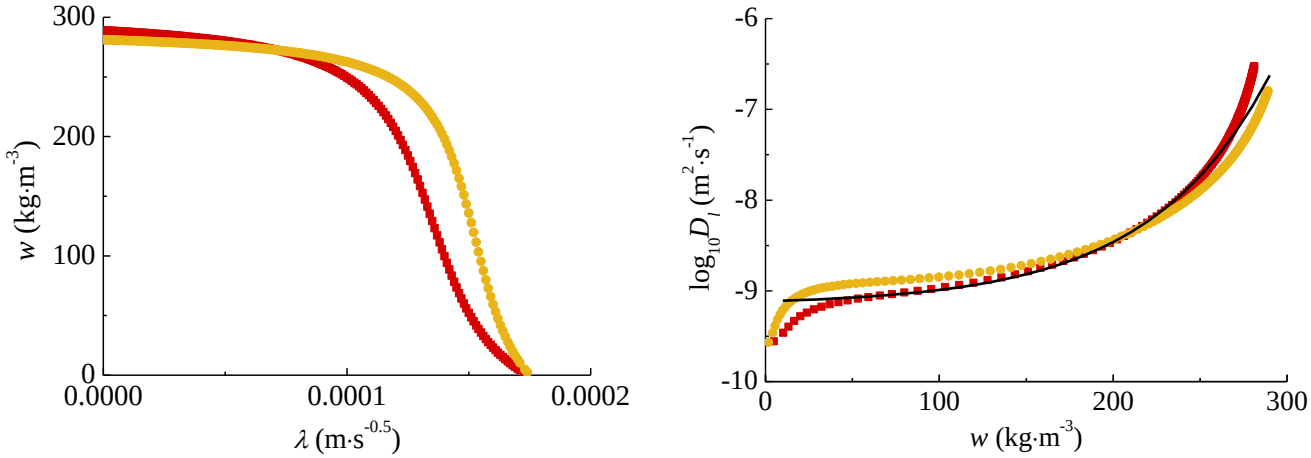

c) The w-λ profile of AAC d) The liquid diffusivity of AAC

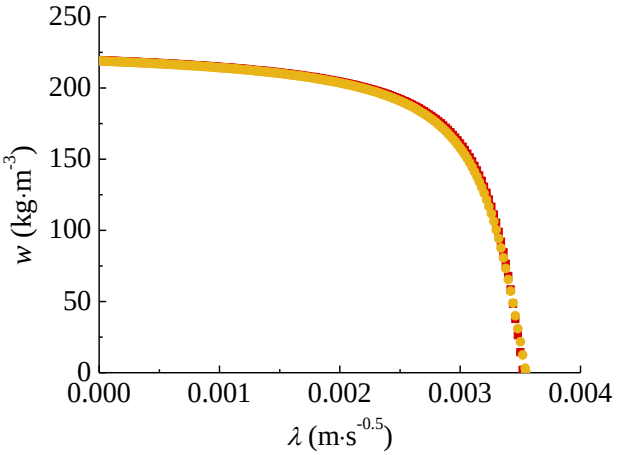

e) The w-λ profile of CB

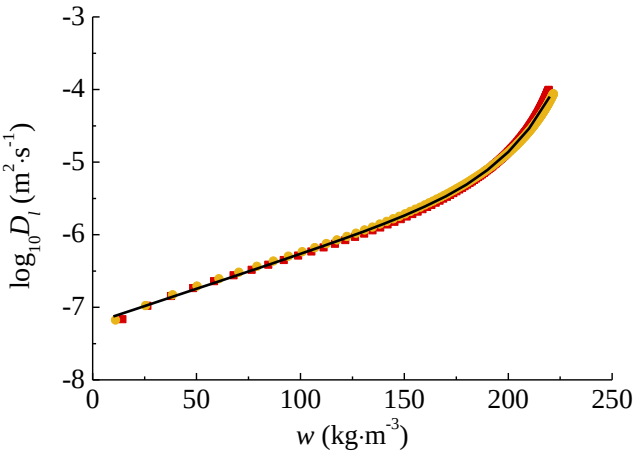

f) The liquid diffusivity of CB

Fig.9 Results of the X-ray attenuation tests

In this campaign, we did not have a second method to validate the reliability of our X-ray test results. However, during the data processing we had the two theoretical constraints that the w-λ profile should intersect the Y-axis at w_{cap}, and that the area enclosed by the w-λ profile and the two axes should equate A_{cap}. Both constraints were met in our case. In addition, the reliability of our X-ray test and data processing had been previously proved by another study, wherein different diffusivity determination methods were used [17].

The last hygric property studied was the liquid permeability, obtained by combining two methods. The liquid permeability for the moisture content above w_{cap} was directly measured by the falling water head test. For lower moisture content, it was calculated according to Eq.(1) with the liquid diffusivity and the moisture retention curve for the absorption process. The overall liquid permeability curve was expressed by Eq.(9). Results are shown in Fig.10 and Table 4.

$$\log_{10} K_l = k_1 + k_2 \cdot w^{k_3} \tag{9}$$

Again, we did not have another test in this campaign to validate the obtained liquid permeability directly. However, with the falling water head setup we had measured the liquid permeability of sintered glass and verified the results by comparison with modeling and with other reported measurements [22, 58]. Thus, the permeabilities of the target materials in this study obtained from direct measurements should be similarly reliable. For the calculated values, Eq.(1) is physically sound. So the calculations could be assumed trustworthy, as long as the liquid diffusivity and the moisture retention curve were reliable. For CS and AAC there was no problem. For CB the absorption moisture retention curve lied above the desorption curve starting from w_{cap}, meaning that its slope close to w_{cap} was overestimated and hence the derived diffusivity from Eq.(1) was underestimated. This explains why the calculated points in Fig.10c were systematically below the fitted curve and failed to connect the direct measurements perfectly. By replacing CB's moisture retention curve for the absorption process with its desorption curve starting from w_{cap}, we obtained the modified results in Fig.10d and Table 4. This way improvement was achieved, but the systematic errors could not be eliminated without the real absorption curve. Fortunately, the deviations were not too large.

To summarize, porous building materials with small pores have high hygroscopicity and are easy for capillary condensation, showing rapid decrease in the vapor diffusion resistance factor as RH increases. Materials with large pores, on the other hand, are high in capillarity with large liquid diffusivity/permeability, especially close to saturation.

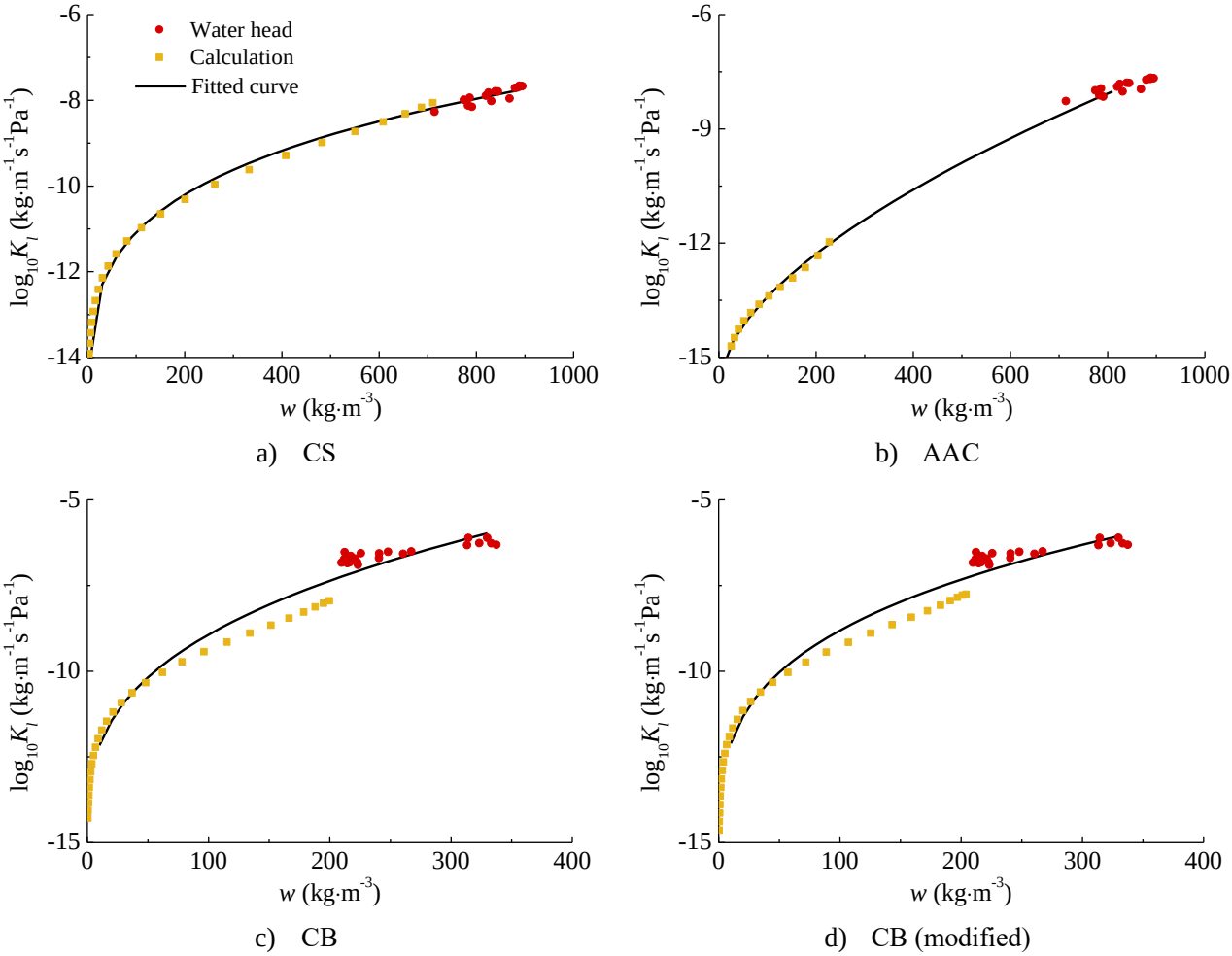

Fig.10 The liquid permeabilities of target materials

Table 4 Fitted moisture transport curves of target materials

Material	Property	k_1	k_2	k_3	k_4	k_5	R^2
CS	μ	0.508	0.252	4.705	-	-	0.92
	D_l (absorption)	$1.40\cdot10^{5}$	$5.61\cdot10^{-4}$	108.9	$-1.40\cdot10^{5}$	$-4.77\cdot10^{7}$	0.98
	K_l	-16.06	1.697	0.234	-	-	>0.99
AAC	μ	0.136	0.324	8.238	-	-	0.99
	D_l (absorption)	-9.15	$1.94\cdot10^{-2}$	69.43	$1.94\cdot10^{-2}$	69.43	0.95
	K_l	-15.67	0.154	0.583	-	-	>0.99
CB	μ	0.0858	0.0169	3.261	-	-	0.40
	D_l (absorption)	$-3.85\cdot10^{4}$	$3.85\cdot10^{4}$	$4.06\cdot10^{6}$	$1.47\cdot10^{-4}$	24.83	>0.99
	K_l	-14.95	1.286	0.335	-	-	0.98
	K_l (modified)	-15.74	1.905	0.280	-	-	0.98

4. Conclusions

This paper determined the hygric properties of three porous building materials – calcium silicate, autoclaved aerated concrete and ceramic brick. In total 12 tests were conducted and the experimental results were reported clearly. Reliable curve fittings were also performed when appropriate. Based on

the test results, the following conclusions are reached:

- The pore size of a material strongly influences its hygric properties. Small pores mainly increase the hygroscopicity (e.g. the sorption isotherms), while large pores primarily enhance the capillarity (e.g. the capillary absorption coefficient). Thus with the information on pore size distribution, it is possible to estimate the overall hygric performance of a material.
- By combining different test methods (the vacuum saturation test, mercury intrusion test, pressure plate test, modified pressure plate test, water column test, semi-permeable membrane test, psychrometer test, desiccator test, capillary absorption test, cup test, X-ray attenuation test and falling water head test), it is possible to reliably obtain the hygric properties of porous building materials in the full humidity range for both absorption and desorption processes.
- Standardized tests are generally dependable but exceptions also exist. For example, if a material mainly consists of large pores (e.g. ceramic brick), low hygroscopicity can be expected and the desiccator test may not be reliable for the determination of its sorption isotherms.
- Newly developed tests (the modified pressure plate test, semi-permeable membrane test and psychrometer test) can be used to obtain the moisture retention curve for the absorption process. But their accuracy close to saturation is limited. Further improvements or innovative methods are needed.
- There is no single method to directly measure the liquid permeability at low and intermediate moisture content. By combining the liquid diffusivity and moisture retention curve for the absorption process, however, it is possible to derive the corresponding liquid permeability.

Acknowledgments

This research is supported by Key Laboratory of New Technology for Construction of Cities in Mountain Area (Project No. LNTCCMA-20200108) and EU H2020 project "RIBuild - Robust Internal Thermal Insulation of Historic Buildings" (No. 637268). Their support is kindly acknowledged.

References

[1] M. Khoukhi, The combined effect of heat and moisture transfer dependent thermal conductivity of polystyrene insulation material: Impact on building energy performance, Energy and Buildings 169 (2018) 228-235.

[2] X. Zhou, J. Carmeliet, D. Derome, Assessment of risk of freeze-thaw damage in internally insulated masonry in a changing climate, Building and Environment 175 (2020) 106773.

[3] S. Ginestet, C. Aschan-Leygonie, T. Bayeux, M. Keirsbulck, Mould in indoor environments: The role of heating, ventilation and fuel poverty. A French perspective, Building and Environment 169 (2020) 106577.

[4] H. Glaser, Graphical method for investigation of diffusional processes, Kaltetechnik 11(10) (1959) 345-349.

[5] ISO 13788: 2012(E) Hygrothermal performance of building components and building elements - Internal surface temperature to avoid critical surface humidity and interstitial condensation: Calculation methods, 2012.

[6] GB 50176-2016 Code for thermal design of civil building (in Chinese), 2016.

[7] D.A. De Vries, Simultaneous transfer of heat and moisture in porous media, Transactions, American Geophysical Union 39(5) (1958) 909-916.

[8] J.R. Philip, D.A. De Vries, Moisture movement in porous materials under temperature gradients, Transactions, American Geophysical Union 38(2) (1957) 222-232.

[9] J.M.P.Q. Delgado, E. Barreira, N.M.M. Ramos, V.P.d. Freitas, Hygrothermal Numerical Simulation Tools Applied to Building Physics, Springer, Berlin, Heidelberg2013.

[10] M. Woloszyn, C. Rode, IEA Annex 41: Whole Building Heat, Air, Moisture Response. Subtask 1: Modeling Principles

and Common Exercises, 2008.
[11] H. Hens, Modeling the heat, air, and moisture response of building envelopes: What material properties are needed, how trustful are the predictions, Journal of ASTM International 4(2) (2007) 1-11.
[12] C. Feng, A.S. Guimarães, N. Ramos, L. Sun, D. Gawin, P. Konca, C. Hall, J. Zhao, H. Hirsch, J. Grunewald, M. Fredriksson, K.K. Hansen, Z. Pavlík, A. Hamilton, H. Janssen, Hygric properties of porous building materials (VI): A round robin campaign, Building and Environment 185 (2020) 107242.
[13] C. Feng, H. Janssen, Hygric properties of porous building materials (IV): Semi-permeable membrane and psychrometer methods for measuring moisture storage curves, Building and Environment 152 (2019) 39-49.
[14] C. Feng, H. Janssen, Hygric properties of porous building materials (II): Analysis of temperature influence, Building and Environment 99 (2016) 107-118.
[15] C. Feng, H. Janssen, Hygric properties of porous building materials (III): Impact factors and data processing methods of the capillary absorption test, Building and Environment 134 (2018) 21-34.
[16] C. Feng, H. Janssen, Y. Feng, Q. Meng, Hygric properties of porous building materials: Analysis of measurement repeatability and reproducibility, Building and Environment 85 (2015) 160-172.
[17] P. Ren, C. Feng, H. Janssen, Hygric properties of porous building materials (V): Comparison of different methods to determine moisture diffusivity, Building and Environment 164 (2019) 106344.
[18] C. Feng, H. Janssen, C. Wu, Y. Feng, Q. Meng, Validating various measures to accelerate the static gravimetric sorption isotherm determination, Building and Environment 69 (2013) 64-71.
[19] M.K. Kumaran, IEA Annex 24: Heat, Air and Moisture Transfer in Insulated Envelope Parts. Final Report, Volume 3, Task 3: Material Properties, 1996.
[20] M.K. Kumaran, A Thermal and Moisture Transport Property Database for Common Building and Insulating Materials, Final Report from ASHRAE Research Project 1018-RP, 2002.
[21] J. Carmeliet, H. Hens, S. Roels, O. Adan, H. Brocken, R. Cerny, Z. Pavlik, C. Hall, K. Kumaran, L. Pel, Determination of the liquid water diffusivity from transient moisture transfer experiments, Journal of Thermal Envelope and Building Science 27(4) (2004) 277-305.
[22] M. Islahuddin, H. Janssen, Pore-Structure-Based Determination of Unsaturated Hygric Properties of Porous Materials, Transport in Porous Media 130(3) (2019) 675-698.
[23] E. Vereecken, S. Roels, H. Janssen, Inverse hygric property determination based on dynamic measurements and swarm-intelligence optimisers, Building and Environment 131 (2018) 184-196.
[24] S. Roels, J. Carmeliet, H. Hens, O. Adan, H. Brocken, R. Czerny, C. Hall, A. Hamilton, K. Kumaran, Z. Pavlik, L. Pel, R. Plagge, F. Tariku, HAMSTAD Work Package 1: Final Report - Moisture Transfer Properties and Materials Characterisation, EU Contract GRD 1-1999-20007, 2003.
[25] M. Fredriksson, P. Johansson, A Method for Determination of Absorption Isotherms at High Relative Humidity Levels: Measurements on Lime-Silica Brick and Norway Spruce (Picea abies(L.) Karst.), Drying Technology 34(1) (2016) 132-141.
[26] C. Feng, H. Janssen, Modified pressure plate method for measuring adsorption moisture retention curves, 12th Nordic Symposium on Building Physics, Tallinn, Estonia, 2020, p. 14004.
[27] M. Fredriksson, E.E. Thybring, On sorption hysteresis in wood: Separating hysteresis in cell wall water and capillary water in the full moisture range, PloS one 14(11) (2019) e0225111.
[28] J. Zhao, R. Plagge, Characterization of hygrothermal properties of sandstones—Impact of anisotropy on their thermal and moisture behaviors, Energy and Buildings 107 (2015) 479-494.
[29] Z. Huang, Y. Sun, F. Musso, Experimental study on bamboo hygrothermal properties and the impact of bamboo-based panel process, Construction and Building Materials 155 (2017) 1112-1125.
[30] B. Haba, B. Agoudjil, A. Boudenne, K. Benzarti, Hygric properties and thermal conductivity of a new insulation material for building based on date palm concrete, Construction and Building Materials 154 (2017) 963-971.

[31] J. Kočí, J. Maděra, M. Jerman, R. Černý, Experimental Determination of Heat and Moisture Transport Properties of AAC in the Range of Subzero to Room Temperatures, International Journal of Thermophysics 40(2) (2019).
[32] M. Jerman, I. Palomar, V. Kočí, R. Černý, Thermal and hygric properties of biomaterials suitable for interior thermal insulation systems in historical and traditional buildings, Building and Environment 154 (2019) 81-88.
[33] B. Seng, C. Magniont, S. Lorente, Characterization of a precast hemp concrete block. Part II: Hygric properties, Journal of Building Engineering 24 (2019) 100579.
[34] T. Colinart, T. Vinceslas, H. Lenormand, A.H.D. Menibus, E. Hamard, T. Lecompte, Hygrothermal properties of light-earth building materials, Journal of Building Engineering 29 (2020) 101134.
[35] ISO 15901-1: 2016(E) Evaluation of pore size distribution and porosity of solid materials by mercury porosimetry and gas adsorption — Part 1: Mercury porosimetry, 2016.
[36] ASTM D4404 - 18: Standard Test Method for Determination of Pore Volume and Pore Volume Distribution of Soil and Rock by Mercury Intrusion Porosimetry, 2018.
[37] ISO 10545-3: 2018 (E) Ceramic tiles - Part 3: Determination of water absorption, apparent porosity, apparent relative density and bulk density, 2018.
[38] ASTM C1699 - 09 (Reapproved 2015): Standard Test Method for Moisture Retention Curves of Porous Building Materials Using Pressure Plates, 2015.
[39] ASTM C642 - 13: Standard Test Method for Density, Absorption, and Voids in Hardened Concrete, 2013.
[40] R.A. Cook, K.C. Hover, Mercury porosimetry of cement-based materials and associated correction factors, Construction and Building Materials 7(4) (1993) 231-240.
[41] ISO 11274: 2019(E) Soil quality - Determination of the water-retention characteristic - Laboratory methods, 2019.
[42] ASTM D6836 - 16: Standard Test Method for Determination of the Soil Water Characteristic Curve for Desorption Using Hanging Column, Pressure Extractor, Chilled Mirror Hygrometer, or Centrifuge, 2016.
[43] R. Plagge, G. Scheffler, A. Nicolai, Experimental methods to derive hygrothermal material functions for numerical simulation tools, Building X Conference, Clearwater, Florida, 2007, pp. 1-12.
[44] ISO 12571: 2013(E) Hygrothermal performance of building materials and products - Determination of hygroscopic sorption properties, 2013.
[45] ASTM C1498 - 04a (2016): Standard Test Method for Hygroscopic Sorption Isotherms of Building Materials, 2016.
[46] ISO 15148: 2002(E) Hygrothermal performance of building materials and products—determination of water absorption coefficient by partial immersion, 2002.
[47] ASTM C1794 - 15: Standard Test Methods for Determination of the Water Absorption Coefficient by Partial Immersion, 2015.
[48] ISO 12572: 2016(E) Hygrothermal performance of building materials and products - Determination of water vapour transmission properties - Cup method, 2016.
[49] ASTM E96 / E96M - 16: Standard Test Methods for Water Vapor Transmission of Materials, 2016.
[50] S. Roels, J. Carmeliet, Analysis of moisture flow in porous materials using microfocus X-ray radiography, International Journal of Heat and Mass Transfer 49(25-26) (2006) 4762-4772.
[51] ISO 17892-11: 2019(E) Geotechnical investigation and testing - Laboratory testing of soil - Part 11: Permeability tests, 2019.
[52] ASTM D2434 - 19: Standard Test Method for Permeability of Granular Soils (Constant Head), 2019.
[53] G.F.B. Sandoval, I. Galobardes, R.S. Teixeira, B.M. Toralles, Comparison between the falling head and the constant head permeability tests to assess the permeability coefficient of sustainable Pervious Concretes, Case Studies in Construction Materials 7 (2017) 317-328.
[54] S. Diamond, Mercury porosimetry: an inappropriate method for the measurement of pore size distributions in cement-based materials, Cement and Concrete Research 30(10) (2000) 1517-1525.

[55] R.J. Good, R.S. Mikhail, The contact angle in mercury intrusion porosimetry, Powder Technology 29(1) (1981) 53-62.
[56] M.T. van Genuchten, A closed-form equation for predicting the hydraulic conductivity of unsaturated soils, Soil Science Society of America Journal 44(5) (1980) 892-898.
[57] C. Evangelides, G. Arampatzis, C. Tzimopoulos, Estimation of Soil Moisture Profile and Diffusivity Using Simple Laboratory Procedures, Soil Science 175(3) (2010) 118-127.
[58] M. Islahuddin, C. Feng, S. Claes, H. Janssen, Validation of pore network model for hygric property calculation, Proceedings of the 4th Central European Symposium on Building Physics. Prague, Czech. MATEC Web of Conference 282, 02024 (2019).

Appendix A Experimental data for the moisture storage of target materials

This appendix illustrates the data points obtained from different methods for the moisture storage curves.

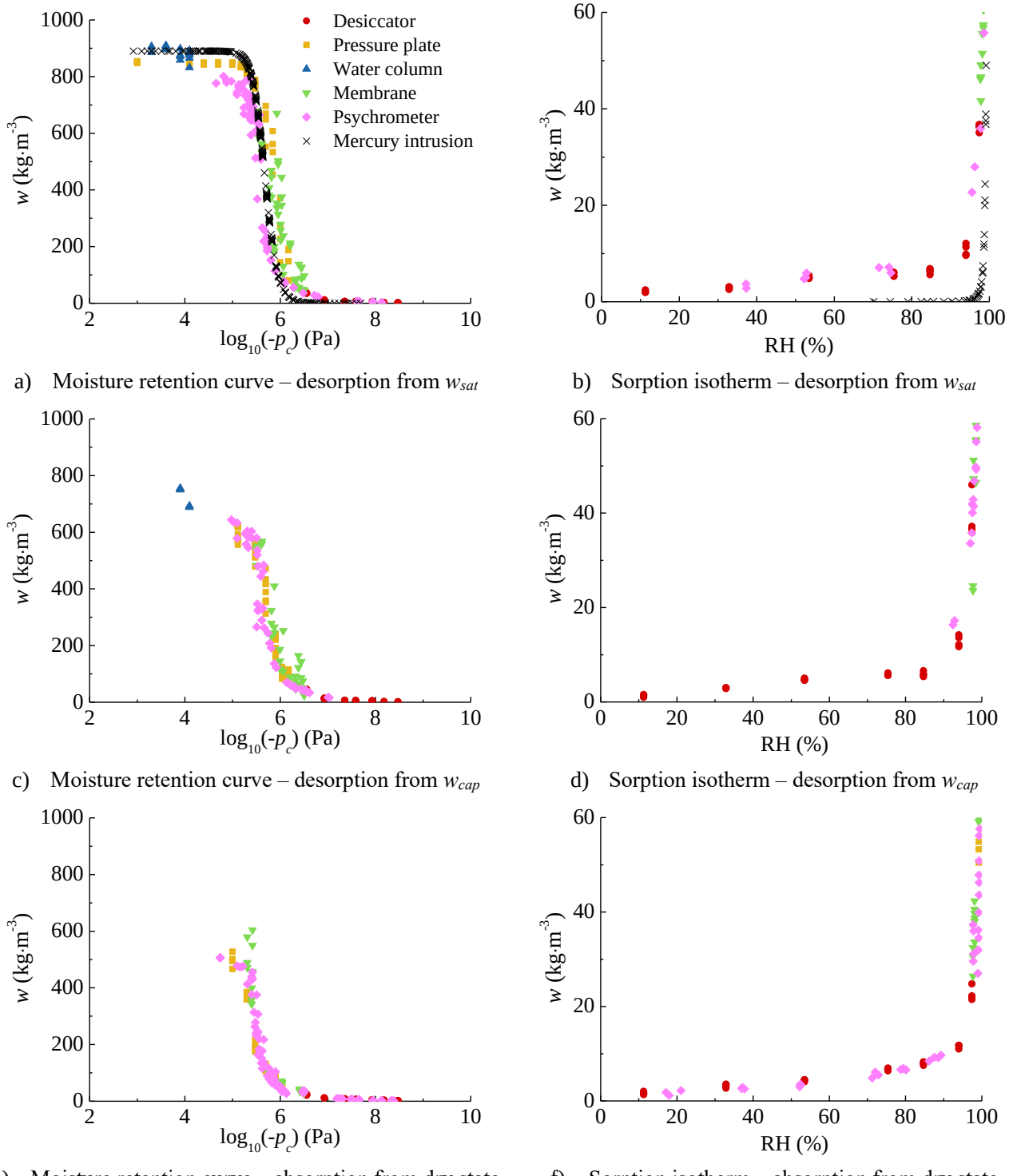

a) Moisture retention curve – desorption from w_{sat}

b) Sorption isotherm – desorption from w_{sat}

c) Moisture retention curve – desorption from w_{cap}

d) Sorption isotherm – desorption from w_{cap}

e) Moisture retention curve – absorption from dry state

f) Sorption isotherm – absorption from dry state

Fig.A1 Experimental results for the moisture storage curves of CS

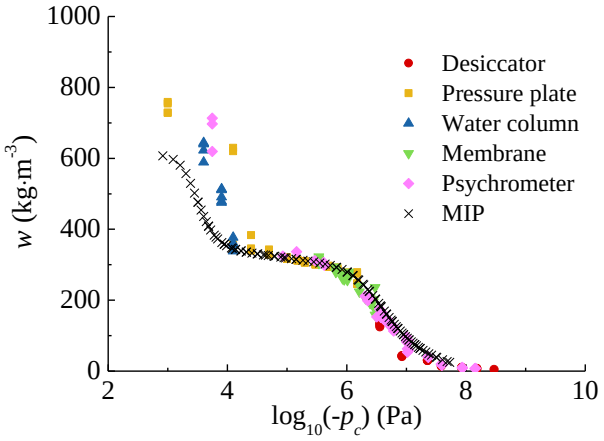

a) Moisture retention curve – desorption from w_{sat}

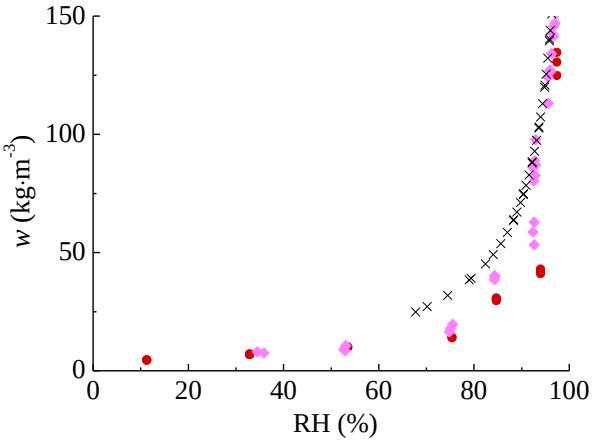

b) Sorption isotherm – desorption from w_{sat}

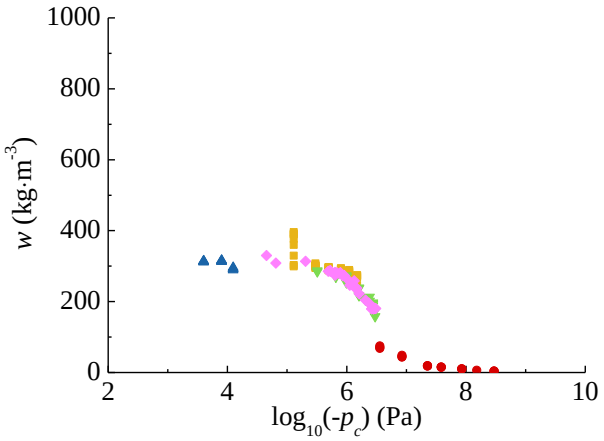

c) Moisture retention curve – desorption from w_{cap}

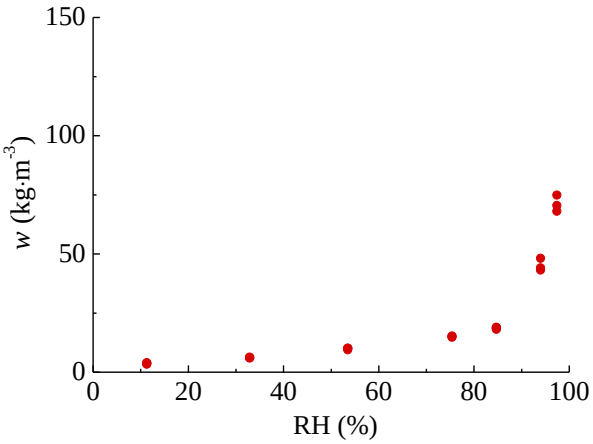

d) Sorption isotherm – desorption from w_{cap}

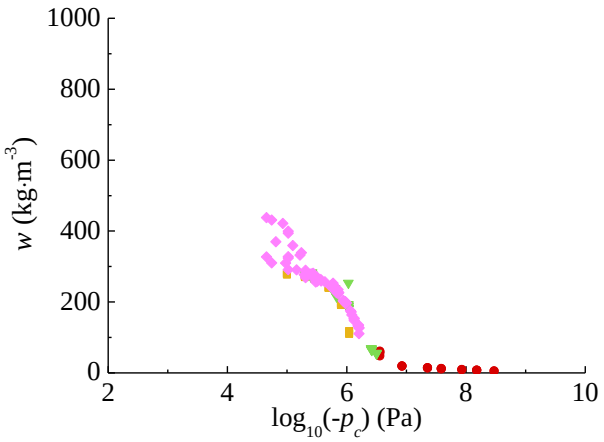

e) Moisture retention curve – absorption from dry state

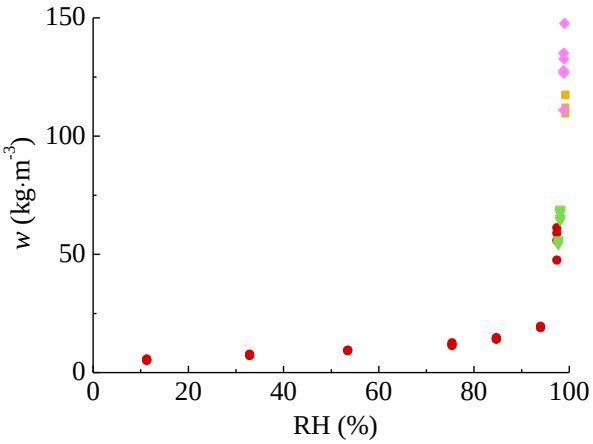

f) Sorption isotherm – absorption from dry state

Fig.A2 Experimental results for the moisture storage curves of AAC

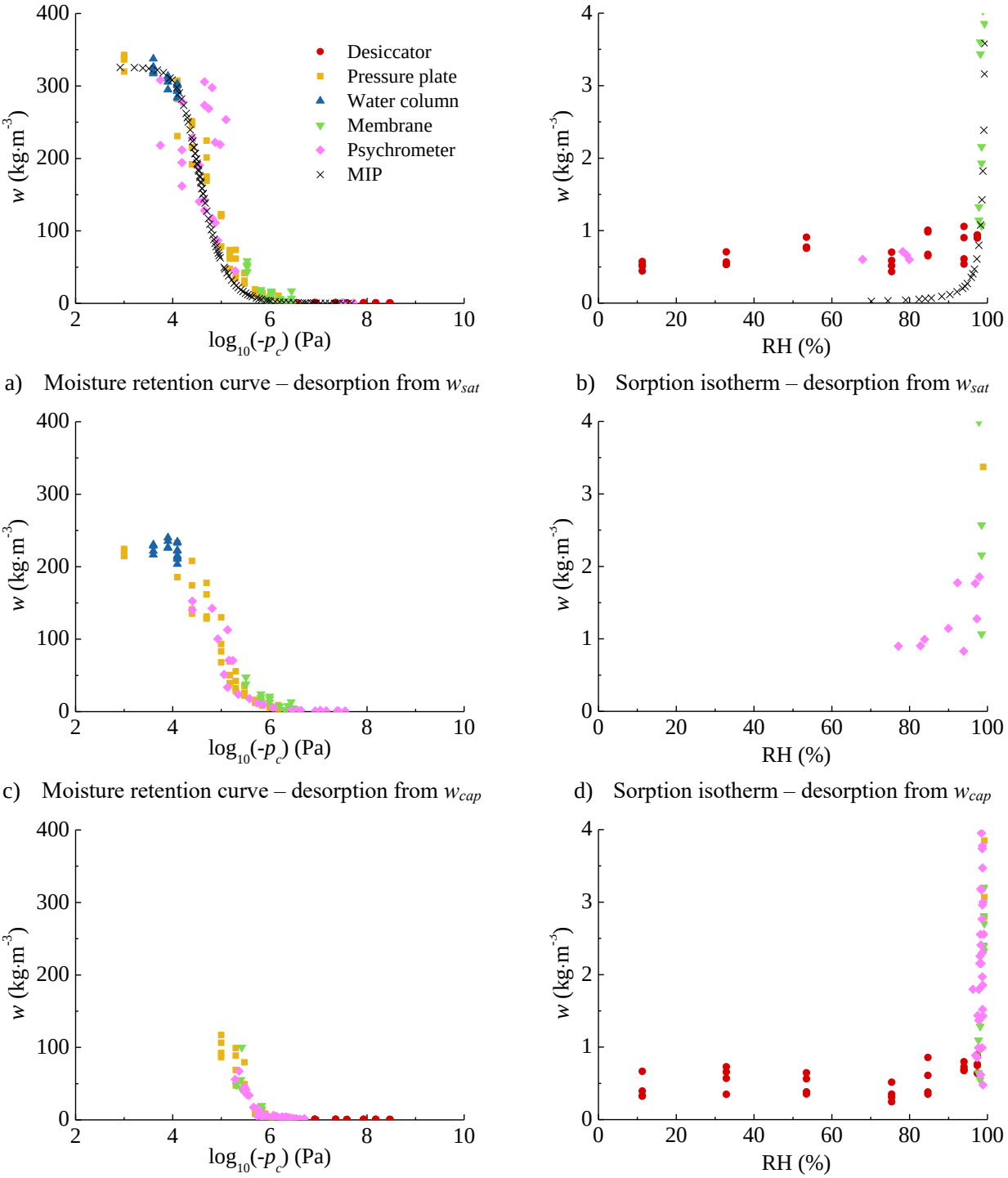

a) Moisture retention curve – desorption from w_{sat}

b) Sorption isotherm – desorption from w_{sat}

c) Moisture retention curve – desorption from w_{cap}

d) Sorption isotherm – desorption from w_{cap}

e) Moisture retention curve – absorption from dry state

f) Sorption isotherm – absorption from dry state

Fig.A3 Experimental results for the moisture storage curves of CB